LAWRENCE
LIVERMORE
NATIONAL
LABORATORY

UCRL-PROC-210798

Nanoscale Twinning and Martensitic Transformation in Shock-Deformed BCC Metals

Luke L. Hsiung

March 24, 2005

MRS 2005 Spring Meeting
San Francisco, CA, United States
March 28, 2005 through April 1, 2005

NANOSCALE TWINNING AND MARTENSITIC TRANSFORMATION IN SHOCK-DEFORMED BCC METALS

Luke L.M. Hsiung, Lawrence Livermore National Laboratory, P.O. Box 808, L-352, Livermore, CA 94551-9900, USA

ABSTRACT

Shock-induced twinning and martensitic transformation in BCC-based polycrystalline metals (Ta and U-6wt%Nb) have been observed and studied using transmission electron microscopy (TEM). The length-scale of domain thickness for both twin lamella and martensite phase is found to be smaller than 100 nm. While deformation twinning of {112}<111>-type is found in Ta when shock-deformed at 15 GPa, both twinning and martensitic transformation are found in Ta when shock-deformed at 45 GPa. Similar phenomena of nanoscale twinning and martensitic transformation are also found in U6Nb shock-deformed at 30 GPa. Since both deformation twinning and martensitic transformation occurred along the $\{211\}_b$ planes associated with high resolved shear stresses, it is suggested that both can be regarded as alternative paths for shear transformations to occur in shock-deformed BCC metals. Heterogeneous nucleation mechanisms for shock-induced twinning and martensitic transformation are proposed and discussed.

INTRODUCTION

The combined effects of high strain rate, high pressure, and high plastic strain on Ta (a group V transition metal) can generate a broad range of microstructural features such as dislocation cells/walls, subboundaries, shear bands, recrystallized grains, and deformation twins... etc. [1-6]. A recent TEM study of deformation substructure developed within shock-deformed tantalum has revealed that shock-induced phase transformation can also take place in tantalum under dynamic pressure conditions [7]. Besides high-density dislocation substructures and deformation twins, plate-like omega phase was also observed in tantalum shock-loaded at 45 GPa as a result of the β (bcc) → ω (hexagonal) displasive or marttensitic transition. The orientation relationships (one variant) between the shock-induced ω and parent β phases are: $(10\bar{1}0)_\omega \parallel (211)_\beta$, $[0001]_\omega \parallel [111]_\beta$, $[1\bar{2}10]_\omega \parallel [0\bar{1}1]_\beta$. The lattice parameters of ω phase are $a_\omega \approx \sqrt{2}\, a_\beta = 0.468$ nm and $c_\omega = (\sqrt{3}/2)a_\beta = 0.286$ nm (c/a = 0.611). It has been well documented that omega phase can be formed in numerous group IV transition metals (titanium, zirconium and hafnium) and their alloys, as well as ordered β-type alloy systems [8-10]. In general, both athermal and isothermal omega phases have been reported [8]. For group IV metals [which have hcp (α) structure at room temperature but transform to bcc (β) structure at high temperatures] athermal to forms either under quenching from the β phase field (i.e. β → ω) or under static and dynamic pressures (i.e. α → ω), whereas isothermal ω forms under high temperature aging (i.e. β → ω). It is noted here that tantalum has a bcc structure and exhibits no phase transformation under ambient and static pressures up to 100 GPa [11, 12]. The occurrence of β → ω transition in tantalum shock-loaded at 45 GPa suggests that the shock-induced phase change involves a non-equilibrium reaction caused by dynamic pressures.

It was proposed that the ω-lattice can be obtained by collapsing one pair of (111) planes within the β-lattice, and leaving the adjacent (111) planes unaltered as schematically illustrated in Fig. 1. The atomic displacements required are $\pm a_o\sqrt{3}/12$, where a_o is the lattice parameter of β-lattice. However, the collapse is not always complete, and it may result in a "rumpled" plane after collapsing. The crystal structure of ideal ω is hexagonal (P6/mmm) if the collapse is complete. Both ideal and rumpled hexagonal contain 3-atoms/unit cell, the equivalent positions are: 0,0,0; 2/3,1/3,1/2; 1/3,2/3,1/2 for ideal hexagonal, and 0,0,0; 2/3,1/3,1/2+z; 1/3,2/3,1/2-z ($0 < z < 0.167$) for rumpled structure. The β-ω phase mixture exhibits unique diffraction patterns [7], which enable it to be easily identified. In general, the ω phase can be identified from the superlattice diffraction spots excited at various $1/3\langle 112\rangle_b$ and $1/3\langle 112\rangle_b$ positions on the $\langle 011\rangle_b$ - and $\langle 113\rangle_b$ -zone patterns of β phase as illustrated in Fig. 2. It has also been proposed previously that similar to the shear mechanism for deformation twinning, i.e. the movements of a homogeneous *1/6*[111] shear in consecutive (211) planes [Fig. 2(a)], omega phase can also be formed displacively by an inhomogeneous shear of *1/12*$\langle 1\bar{1}\,\bar{1}\rangle$, *1/3*$\langle 1\bar{1}\,\bar{1}\rangle$, and *1/12*$\langle 1\bar{1}\,\bar{1}\rangle$ in consecutive $\{211\}_\beta$ planes [Fig. 2(b)]. The omega sequence caused by the three-layer inhomogeneous shear is equivalent to the atomic shuffling of ±*1/12*$\langle 1\bar{1}\,\bar{1}\rangle$ in a pair of {211} planes, which transforms the bcc lattice to

an omega lattice based upon the collapse model shown in Fig. 1. The shock-induced $\beta \rightarrow \omega$ displacive transition can therefore be regarded as a martensitic transformation.

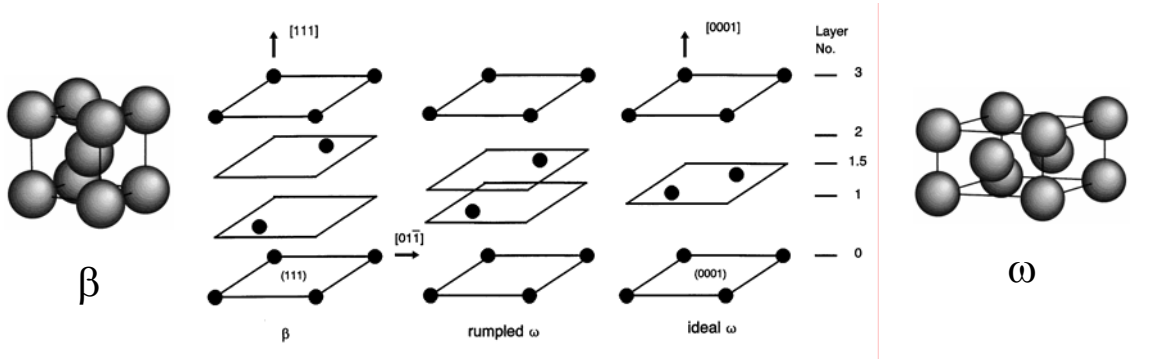

Fig. 1. Lattice correspondence between β (bcc) and rumpled ω and ideal ω phases based upon the (111)-plane collapse model. The ω-lattice can be obtained by collapsing one pair of (111) planes within β-lattice.

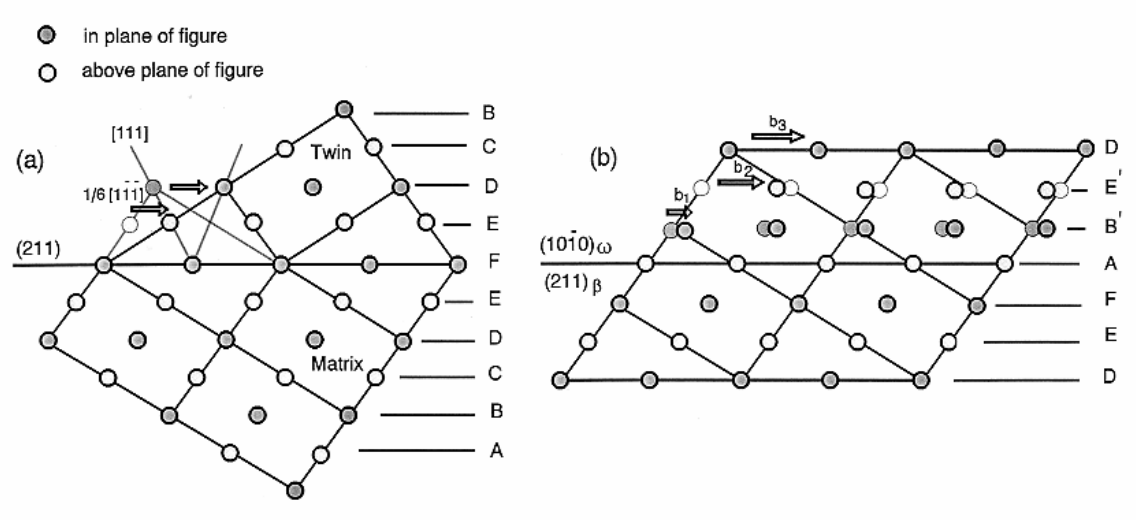

Fig. 2. (a) deformation twinning due to a consecutive shear of $1/6[1\bar{1}\,\bar{1}]$ in the $(211)_{matrix}$ plane, and (b) $\beta \rightarrow \omega'$ transition due to a consecutive shear of $1/12[1\bar{1}\,\bar{1}]$, $1/3[1\bar{1}\,\bar{1}]$, and $1/12[1\bar{1}\,\bar{1}]$ in the $(211)_\beta$ plane; $\mathbf{b}_1$, $\mathbf{b}_2$ and $\mathbf{b}_3$ are translation vectors of $1/12[1\bar{1}\,\bar{1}]$, $1/12[1\bar{1}\,\bar{1}] + 1/3[1\bar{1}\,\bar{1}]$, and $1/12[1\bar{1}\,\bar{1}] + 1/3[1\bar{1}\,\bar{1}] + 1/12[1\bar{1}\,\bar{1}]$, respectively.

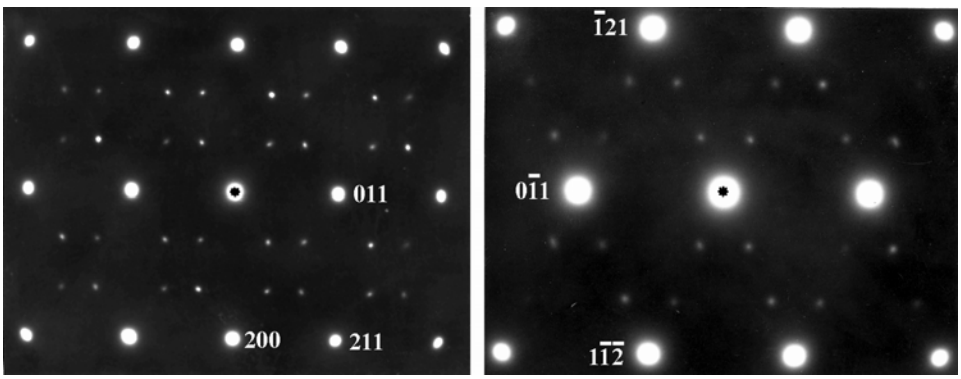

Fig. 3. Diffraction patterns showing lattice correspondence between ω phase and β matrix, (a) $[1\bar{2}10]_{\omega'} \parallel <0\bar{1}\,1>_\beta$ and (b) $[1\bar{2}13]_{\omega'} \| <311>_\beta$. The spots appeared at various $1/3<112>_\beta$ and $2/3<112>_\beta$ positions in (a) and (b) are corresponding to the ω phase of two different *variants*.

EXPERIMENTAL DETAILS

Ingot metallurgy (IM) tantalum in the form of plate stock was obtained from Cabot Corporation, Boyerstown, PA and was produced using a standard electron-beam melt process. The interstitial impurities in this test material are, in parts per million (ppm), oxygen: 23; nitrogen: 20; hydrogen: 1.3; carbon: < 2. A single explosively driven shock-recovery experiment was performed in which cylindrical samples of 5mm thick, 40 mm in diameter were used for the test and the loading axis is parallel to the cylindrical axis. The calculated peak shock pressure and duration for the shock-recovery test were 45 GPa and 1.8 μs, respectively. The microstructures of shock-recovered tantalum were examined using a JEOL-200CX transmission electron microscope equipped with a double-tilt goniometer stage. TEM foils were sliced from a shocked cylindrical sample with the foil normal inclined approximately 45° with respect to the loading axis. TEM specimens were finally prepared by a standard twin jet electropolishing technique in a solution of 94 vol.% methanol, 5 vol.% sulfuric acid and 1 vol.% hydrofluoric acid at -25 V and -20°C. A cast U-6wt%Nb alloy was originally fabricated from Rocky Flats. It was VAR-VAR cast and wrought processed to the final shape of plate (~32 mm thick). The average grain size of the alloy is about 120μm. A single explosively driven shock-recovery experiment was conducted by detonating explosive on one side of the flat plate. The loading axis is perpendicular to the surface plane of the plate, and the calculated peak pressure and peak duration were 30 GPa and 1.5 μs, respectively. Thin foils for TEM observation were prepared by a standard procedure, which included slicing, grinding, and polishing the recovered fragments with the foils surface approximately perpendicular to the loading axis. Final thinning of the foils was performed by a standard twinjet electropolishing technique in an electrolyte (59% methanol, 35% butyl Cellosolve, and 6% perchloric acid) at ~25 V and at a temperature between 0 and -10 $^{\circ}$ C.

DISCUSSION

Shock-induced nanoscale twinning and omega phase in Ta

Figure 4 (a) is a bright-field TEM image showing a heavily jogged, kinked, and tangled dislocation substructure within a Ta sample shocked at 15 GPa. Figure 4(b) is a dark-field TEM image shows several twin bands of 50 nm to 100 nm thick were also formed within the Ta sample. The selected-area diffraction pattern generated from the area in Fig. 4(b) is shown in Fig. 4(c), in which the diffraction spots corresponding to the twin bands are indexed by arrows.

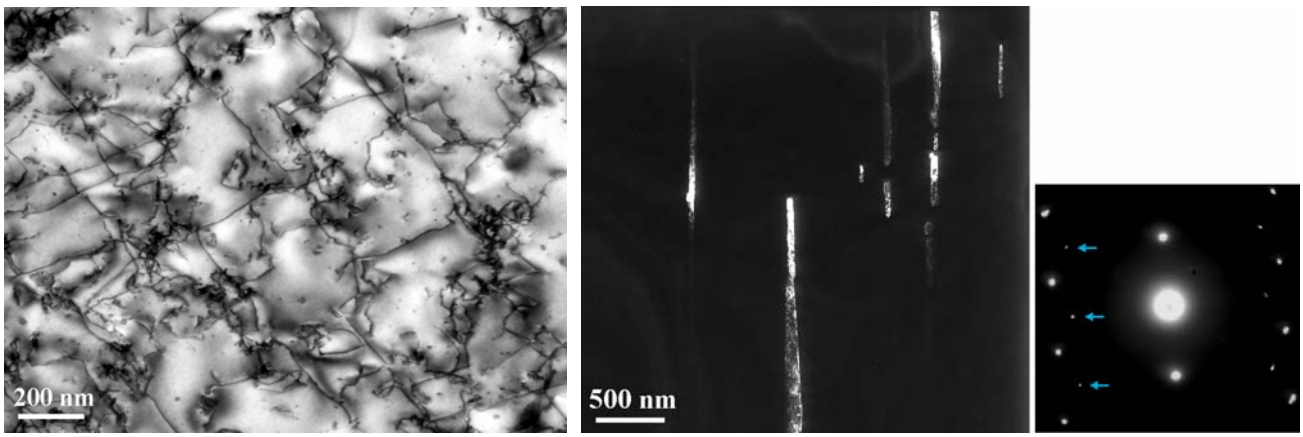

(a) (b) (c)

Fig. 4. (a) A bright-field TEM image showing a heavily jogged, kinked, and tangled dislocation structure within a Ta sample shocked at 15 GPa. (b) A dark-field TEM image showing the formation of nanoscale twin bands within the shocked Ta. (c) A selected-area diffraction pattern generated from the area shown in (b), in which the diffraction spots corresponding to the twin bands are indexed by arrows.

Figure 5(a) is a dark-field TEM image showing the formation (211)-type twin bands of ~10 nm thick in a recovered tantalum sample shocked at 45 GPa. In addition of nanoscale twin bands, some fine and irregular shaped ω plates embedded with a high density dislocation structure were also observed within the shock-recovered Ta sample [see Figs. 6 (a) and (b)]. Figure 6 (c) shows a selected-area diffraction pattern of $<311>_{\beta}$-zone generated from the area in (a). Here, extra diffraction spots corresponding to ω phase were excited at 1/3 $<121>_{\beta}$ and 2/3 $<121>_{\beta}$ positions. Figure 7 shows the coexistence of nanoscale twin domains with fine ω plates observed within the shock-recovered Ta sample. Here, omega phase and twin domain can be readily distinguished by the inset <011>-zone diffraction patterns.

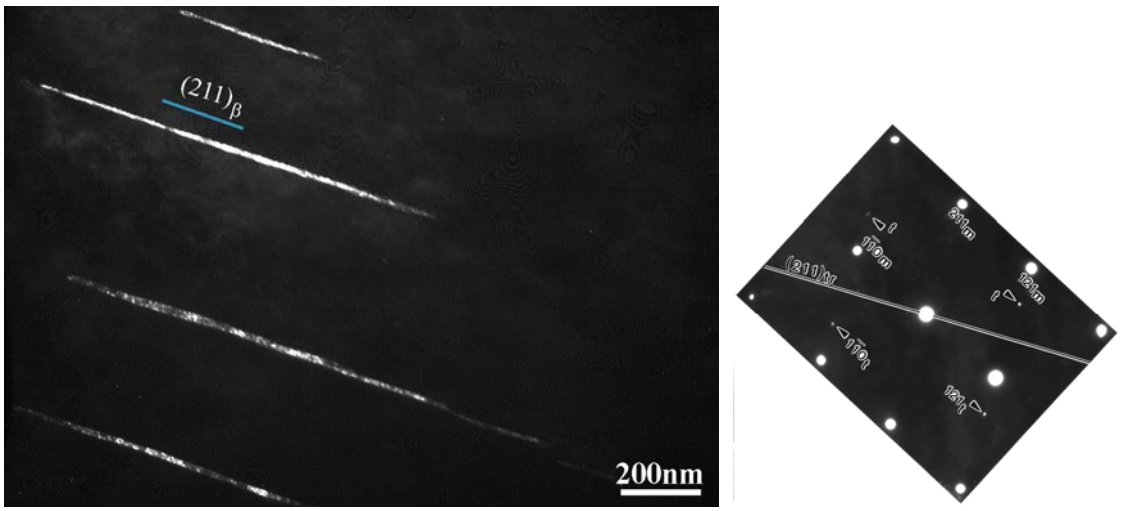

(a) (b)

Fig. 5. (a) A dark-field TEM image showing the {211}-type nanoscale twin bands in Ta shocked at 45 GPa. (b) Selected-area diffraction pattern generated from the area in (a), in which the diffraction spots corresponding to the twin bands are indexed by arrows.

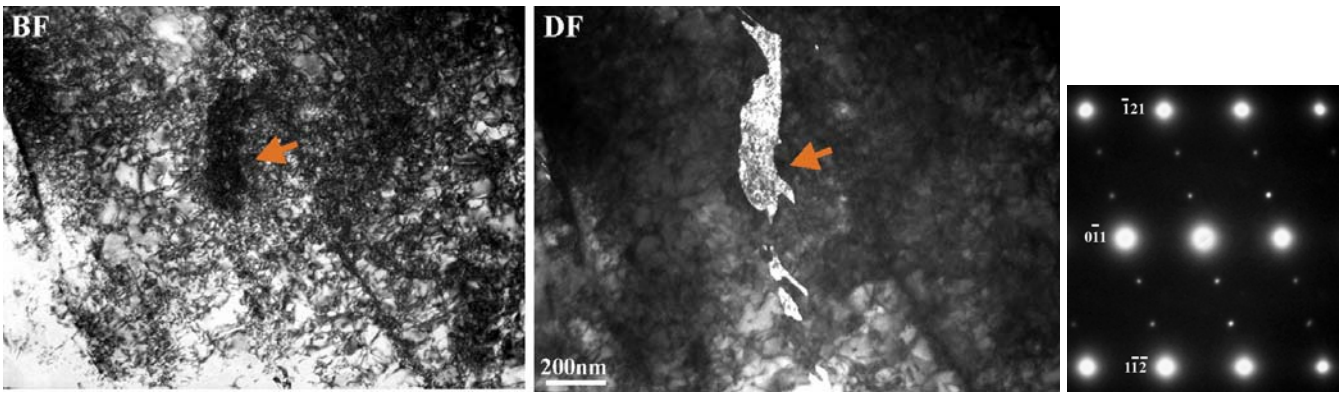

(a) (b) (c)

Fig. 6. (a) A bright-field TEM image, (b) a dark-field TEM image, and (c) a selected-area diffraction pattern of <311>-zone showing the formation of shock-induced ω phase (marked by an arrow) within Ta shocked at 45 GPa.

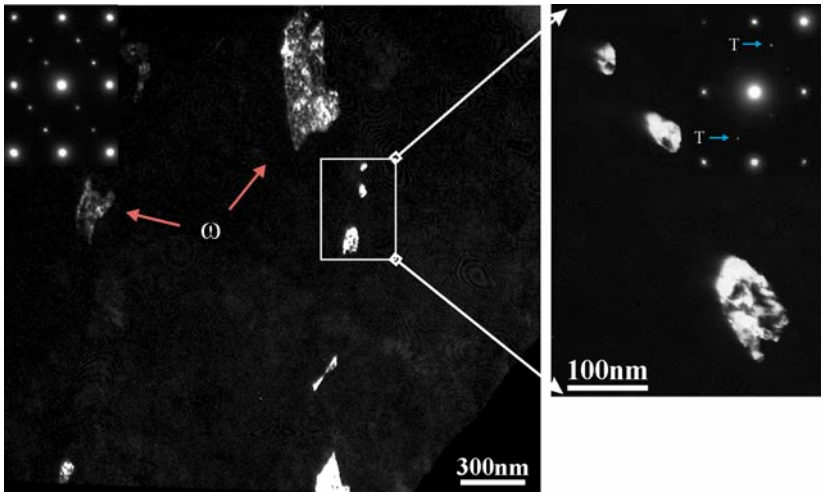

(a) (b)

Fig. 7. Dark-field TEM images of (a) an overview and (b) a higher magnification view of the specified region in (a) showing the coexistence of nanoscale twin domains with fine ω plates within Ta shocked at 45 GPa. Note that diffraction spots corresponding to the nanoscale twin domains are marked by arrows.

Shock-induced nanoscale twinning and omega phase in U-6wt%Nb

Similar shock-induced deformation substructures observed in Ta are also found in cast U-6wt%Nb, which has a BCC (γ) structure. Figure 8 shows a set of dark-field TEM images obtained by using various diffraction spots of the [012]-zone diffraction pattern to image. The diffraction pattern was generated from an area containing nanoscale twin bands of the {211}-type. The twin bands appered as a bright contrast in the upper left image become invisible in the lower left image when a matrix spot is used for imaging. It is of interest to note that twin bands of thickness as small as 1 nm are observed. Also notice the collision of two twin bands at site C.

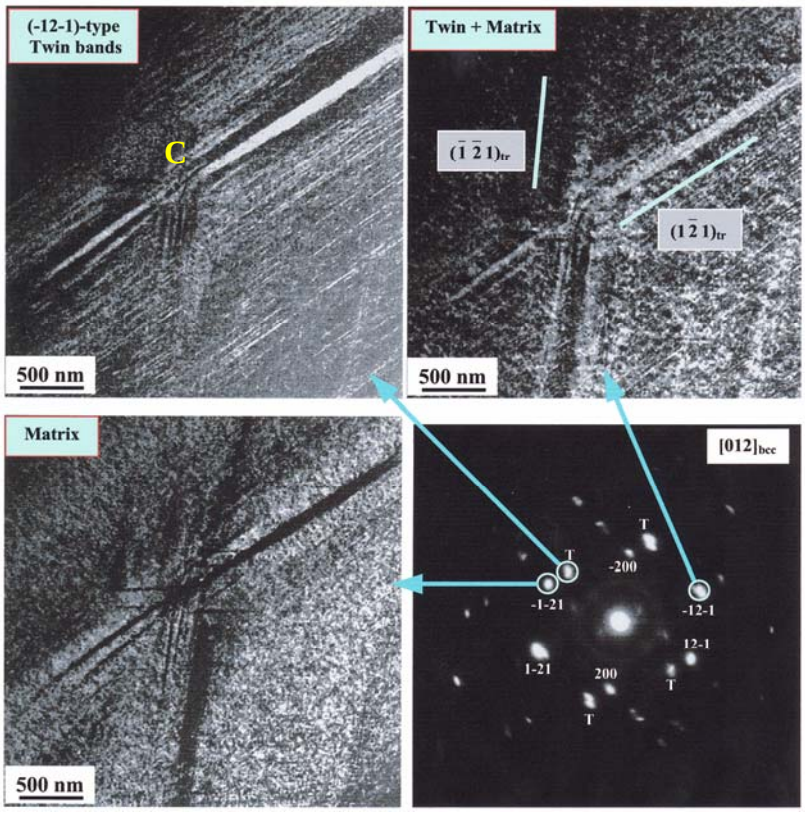

Fig. 8. A set of dark-field TEM images showing the formation of nanoscale twin bands in a shock-deformed U-6wt%Nb sample.

The formation of nanoscale ω-like bands is evidence in Fig. 9, in which a series of dark-field images obtained by using various diffraction spots of the [011]-zone diffraction pattern. Notice that extra diffraction spots corresponding to ω-like phase were excited at various 1/3 $<112>_\gamma$ and 2/3 $<112>_\gamma$ positions. The ω-like phase appered as a bright contrast becomes invisible in the upper right image when a matrix spot is used for imaging.

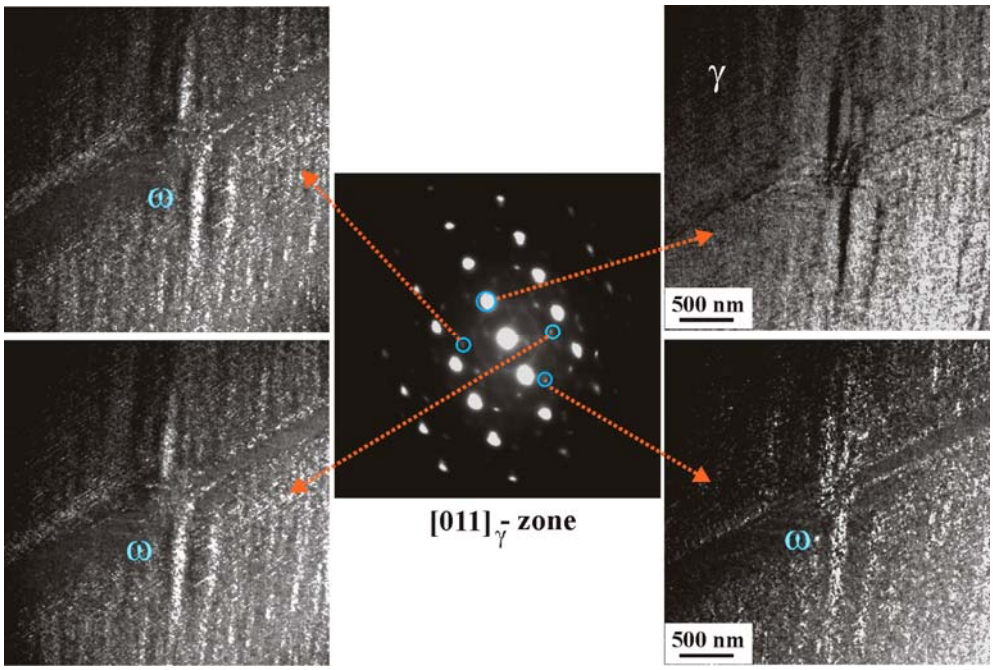

Fig. 9. A set of dark-field TEM images showing the formation of nanoscale twin bands in a shock-deformed U-6wt%Nb sample.

Heterogeneous nucelation mechanisms for shock-induced twinning and martensitic transformation

It has been shown in Fig. 2 that the shear operations for the alteration of bcc structure to twin and omega domains can be produced by the glide of partial dislocations of the type *1/3*[111], *1/6*[111] and *1/12*[111] dissociated from the ½[111] perfect dislocations. Figure 10 (a) illustrates the schemes for the dissociation of ½<111> dislocation for twinning and omega transformation based upon a zonal dislocation model described in [13]. Each ½[111] dislocation can dissociate into three *1/6*[111] partials (each one plane apart) to form a three-layered twin domain and leave a zonal dislocation with no net Burgers vector. Accordingly, it requires the dissociation of two ½[111] dislocations with two-plane apart to form a unit (six-layer) twin domain. Similarly, the partial dislocations for omega transformation can be obtained by the dissociation of a ½[111] dislocation into two *1/12*[111] partials and one *1/3*[111] partial (each one plane apart) to form a unit (three-layer) omega domain and leave a zonal dislocation with no net Burgers vector. The above two dissociation reactions, i.e. $\mathbf{b} \rightarrow \mathbf{b_1} + \mathbf{b_2} + \mathbf{b_3}$, are energetically feasible because the free energy is gained in the process according to Frank's criterion: $b_1^2 + b_2^2 + b_3^2 < b^2$.

In reality, it is very difficult to form a dislocation structure with dislocation lines only two-plane apart (0.27 nm) in {211}. However, it is highly possible that screw dislocation lines contain many atomic jogs [jog height (d) = 0.27 nm], which are either grown-in thermal jogs or generated by dislocation intersection during the onset of shock deformation. Accordingly, it is highly possible that under dynamic pressure conditions, dislocation loops can bow out in groups from many line segments along a screw dislocation line to form dislocation aggregate as illustrated in Fig. 10 (b), which has been practically observed and shown in Fig. 10 (c). Twin and omega domains can thus be nucleated heterogeneously at the hatched area in Fig. 10 (b), in which many dislocation loops are overlapping one

another that cause a mechanical instability to occur and in turn facilitate the reactions of dislocation dissociation proposed in Fig. 10(a). It is worth noting that the elliptical dislocation aggregates resulted from the overlapped dislocation loops are more likely to form when the motion of screw dislocations are further restricted, i.e. $v_s << v_e$. Consequently, edge dislocation segments become the major carriers for plastic strain. Since the edge dislocation segments can only move parallel to the <111>-direction, more overlapping is resulted among the dislocation loops. Furthermore, since the friction stress or resistance for *1/3*<111> anti-twinning dislocation is greater than that for *1/6*<111> twinning dislocation [14], the growth of omega domain controlled by the movement of *1/3*<111> dislocations is expected to be slower than that of twin domain controlled by the movement of *1/6*<111> dislocations. As a result, the length of twin domain is usually much longer than that of omega domain.

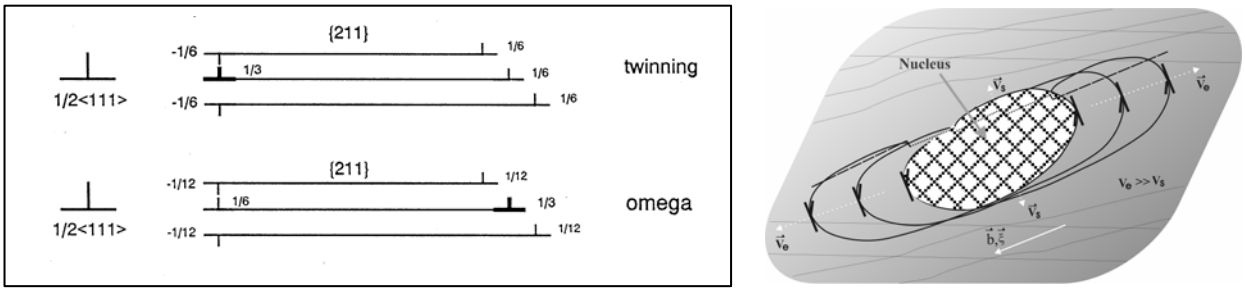

(a) (b)

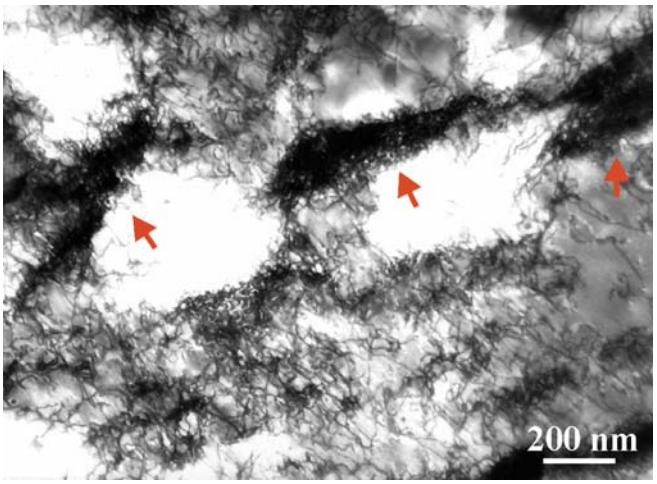

(c)

Fig. 10. (a) A schematic representation of zonal dislocation models for the core dissociation of ½[111] perfect dislocation corresponding to deformation twinning and omega transformation, respectively. For simplicity, the partials *1/3*[111], *1/6*[111], and *1/12*[111] are respectively designated simply *1/3*, 1/6, and *1/12*; (b) The formation of dislocation agglomerate from a jogged screw dislocation, where twin or omega phase can be nucleated from the hatched area depending on the dislocation core dissociations proposed in (a). Here, v_s, v_e, l, d, $\vec{\mathbf{b}}$, and $\vec{\xi}$ denote velocities of screw dislocation, edge dislocation, free segment length, jog height, Burgers vector, and line vector respectively. (c) The observation of dislocation aggregates or clusters (marked by arrows) in Ta shocked at 45 GPa.

CONCLUSION

Nanoscale twinning and martensitic transformation have been observed within shock-deformed Ta and U-6wt%Nb. Both deformation twins and shock-induced ω phase are primarily formed along the {211) planes. It is suggested that shear deformation in the {211) planes is the major cause for the

formation of shock-induced ω phase. Heterogeneous nucleation mechanisms based upon the dislocation clustering accompanied with the core dissociation of ½<111> into three *1/6*<111> twinning dislocations, and *1/12*<111>, *1/3*<111> and *1/12*<111> transformation dislocations are proposed to rationalize the shock-induced twinning and martensitic transformation. Owing to the relatively lower mobility of *1/3*<111> anti-twinning dislocation than *1/6*<111> twinning dislocation, the average length of shock-induced ω domain is much shorter than that of shock-induced twin domain.

ACKNOLEDGEMENTS

This work was performed under the auspices of the U. S. Department of Energy by the University of California, Lawrence Livermore National Laboratory under Contract No. W-7405-Eng-48.

REFERENCES

1. J. C. Huang and G. T. Gray III, Acta Metall. 37, 3335 (1989).
2. L. E. Muff, C.-S. Niou, S. Pappu; J. M. Rivas, and S. A. Quinones, Phys. Stat. Solids A. 149, 253 (1995).
3. L. E. Murr, M. A. Meyers, C.-S. Niou, Y. J. Chen, S. Pappu, and C. Kennedy, Acta Mater. 45, 157 (1997).
4. V. F. Nesterenko, M. A. Meyers, J. C. LaSalvia, M. P. Bondar, Y. J. Chen, and Y. L. Lukyanov, Mater. Sci. Eng. A229, 23 (1997).
5. C. L. Briant, R. H. Batcheler, D. H. Lassila, and W. Gourdin, in Tantalum, edited by Chen et al., p. 191, TMS, Warrendale, PA (1996).
6. D. H. Lassila and G. T. Gray III, J. Phys. IV, Colloque C3, 1, C3-19 (1991).
7. L. M. Hsiung and D. H. Lassila, Acta Mater. 48, 4851 (2000).
8. S. K. Sikka, Y. K. Vohra, and R. Chidambaram, Progr. Mater. Sci. 245 (1982).
9. S. Banerjee and R. W. Cahn, Acta Metall. 31, 1721 (1983).
10. L. A. Bendersky, W. J. Boettinger, B. P. Burton, and F. S. Biancaniello, Acta Metall. Mater. 38, 931 (1990).
11. D. A. Young, Phase Diagrams of the Elements, University of California Press, Berkeley: California, 1991.
12. E. Yu Tonkov and E. G. Ponyatovsky, Phase Transformations of Elements under High Pressure, CRC Press, 2005.
13. J. P. Hirth and J. Lothe, Theory of Dislocations (2nd edition), J. Wiley, New York, 1981.
14. V. Vitek, *Crystal Lattice Defects*, **5**, 1 (1974).